IRAQI JOURNAL OF MATERIALS
Volume (4) Issue (3) July-September 2025, pp. 109-114

Air Purification System Based on Photocatalytic Activity of TiN:TiO_2 Thin Film Nanocomposites

Firas J. Kadhim, Mays K. Ali

Department of Physics, College of Science, University of Baghdad, Baghdad, IRAQ

Abstract
This study investigates the fabrication of titanium dioxide:titanium nitride (TiO_2/TiN) nanocomposite films and their application in enhancing photocatalytic efficiency for air purification, specifically targeting methane (CH_4) gas contamination. The nanocomposites were synthesized via dc reactive magnetron sputtering of a high-purity titanium target in the presence of optimized oxygen and nitrogen gas mixtures. Characterization of the as-prepared nanocomposites included analysis of their structural, morphological, and optical properties. The primary objective of this research was to augment the photocatalytic activity of these nanocomposites against CH_4 pollution. We observed a direct correlation between increased nitrogen content within the TiO_2/TiN nanocomposite structure and significant improvements in photocatalytic efficiency. Under UV irradiation, these nanocomposites demonstrated enhanced methane removal from the ambient air, substantiating the beneficial effect of elevated nitrogen incorporation. These findings suggest the substantial promise of TiO_2/TiN nanocomposites for the remediation of harmful gases and pollutants in both indoor and outdoor environments. This work not only highlights the considerable potential of TiO_2/TiN nanocomposites for air purification but also underscores the significance of advanced synthesis techniques, such as dc reactive magnetron sputtering, in materials science, engineering, and environmental remediation.

Keywords: Nanocomposites; Titanium dioxide; Titanium nitride; Air purification
Received: 23 March 2025; **Revised:** 03 May 2025; **Accepted:** 17 May 2025; **Published:** 1 July 2025

1. Introduction

In the relentless pursuit of cleaner and safer environments, advanced materials and innovative technologies have become pivotal in addressing the challenges posed by harmful gases and pollutants in our atmosphere [1]. One promising avenue of research in this realm revolves around the utilization of photocatalytic materials for air purification, with titanium dioxide (TiO_2) emerging as a frontrunner due to its exceptional photocatalytic properties. The significant attention of TiO_2 as a photocatalyst due to its well-documented properties. These attributes encompass chemical stability, exceptional photocatalytic activity, the capability to be deposited as thin films, and its eco-friendliness [2]. TiO_2 exists in three distinct polymorphs, among them, rutile and anatase TiO_2 are the most stable forms. Rutile TiO_2 possesses a direct bandgap, while anatase TiO_2 features an indirect bandgap of 3.2 eV [3].

There are several methods used to prepare titanium dioxide thin films, such as spray pyrolysis [4], vacuum-based thermal evaporation [5], radio-frequency sputtering [6], and dc reactive magnetron sputtering [7]. Despite the relatively higher costs associated with sputtering techniques conducted in a high vacuum environment, these methods remain highly relevant and widely utilized in various fields. This enduring importance can be attributed to the reasonably high purity of the final product, the nanostructured characteristics of the films, and their exceptional uniformity [8]. This method is also optimum for preparation of thin films with tailored properties. DC sputtering provides precise control over film thickness, composition, and crystallinity. Its capability to control the content of various components within the film is crucial, as it allows researchers to fine-tune the photocatalytic behavior of TiO_2 thin films, thus optimizing their performance in air purification applications [9].

Photocatalyst materials have demonstrated their utility in diverse fields, including water purification [10], self-cleaning surfaces [11], and renewable energy generation [12]. However, their role in gas purification stands out as a pressing need in our ever-polluted world, making the advancements in TiO_2 thin films [13].

Pure TiO_2 films possess a wide bandgap, limiting their responsiveness to UV light, which is a drawback in the context of photocatalytic applications [14]. To enhance their photocatalytic effectiveness, various techniques have been employed to extend their light absorption to the visible spectrum. Among these methods, one of the most widely adopted approaches involves converting TiO_2

into nanoparticles [15-20]. Numerous strategies have been devised for this purpose, including the introduction of dopants such as metals, non-metals (e.g., nitrogen), and semiconductors [21,22].

Notably, substitutional doping with nitrogen has emerged as the most successful approach. This is because the p states of nitrogen atoms blend with the O_2p states, leading to a narrowing of the TiO_2 bandgap. In contrast, although sulfur (S) doping can also achieve a comparable bandgap reduction, its relatively large ionic radius poses challenges when attempting to incorporate it into the TiO_2 crystal lattice. This is evident from the considerably higher formation energy required for the substitution of sulfur compared to nitrogen atoms [23].

In this work, TiO_2:TiN nanocomposite thin films were prepared by dc reactive sputtering with different contents of nitrogen. These nanocomposite thin films were employed in air purification application as the methane gas was used as a pollution sample. Through a comprehensive understanding of the possible enhancement in photocatalytic activity, we aim to shed light on the promising future of air purification technologies and the vital role that TiO_2:TiN thin films play in this quest for cleaner and healthier environments.

2. Experimental Work

Titanium dioxide:Titanium nitride (TiO_2:TiN) nanocomposite thin film were deposited on glass substrates by dc reactive magnetron sputtering technique using different mixing ratios of argon, oxygen and nitrogen gases. In a typical experimental setup, a magnetron sputtering configuration was employed for the preparation of these thin film samples using high-purity 8cm-diameter titanium sheet mounted on the cathode. The inter-electrode distance was maintained at 4 cm and the deposition time lasted for 3 hours. The employment of magnetron at the cathode assists in increasing the confinement of electron near the surface of the cathode and hence increase the rate of collisions and consequently the sputter yield. Also, the employment of magnetron at the anode assists to produce homogeneous deposition on the substrate. As a result, most properties of the deposited material can be reasonably enhanced due to the higher sputter yield and homogeneous distribution of particles on the substrate.

The substrate was heated up to 200°C throughout a controlled heating system to induce better formation of composite structure. The ratios of the reactive gases, oxygen and nitrogen, were varied to produce the TiO_2/TiN nanocomposite film with different contents of TiN. The structural, morphology and optical properties of the deposited films were determined by x-ray diffraction (using Shimadzu XRD 6000 diffractometer), field-emission scanning electron microscopy (FE-SEM) and energy-dispersive x-ray spectroscopy (EDX) (using JSM-7600F JEOL instrument), Fourier-transform infrared spectroscopy (using Shimadzu 16442 FTIR spectrometer), and UV-visible spectrometry (using KMAC SP-8001 spectrophotometer).

The experimental setup used for gas purification efficiency measurements contains a cylindrical chamber with 6 cm diameter and 30 cm length with a gas injection port. Inside the chamber, a 20cm-long 100W ultraviolet (UV) light source is positioned along the axis parallel to the cylinder's axis. This source emits light spectrum centered at 300 nm, as illustrated in Fig. (1). An MQ2 sensor is installed inside the chamber. 20 glass slides (each has 2.5x7.5cm^2 dimensions) upon which the nanocomposite films have been previously deposited, are maintained on the inner wall of the cylinder at a distance of 3 cm from the UV source. The total area covered by these slides is approximately 680 cm^2. The sensor is connected to a pre-programmed Arduino card, which, in turn, interfaces with a display screen showing the gas concentration in ppm units. The displayed concentration is calibrated according to the type of gas being analyzed. The entire system is connected to a personal computer for real-time data recording during the examination, as depicted in Fig. (1). The experiment was carried out at room temperature (~27°C). The pressure inside the chamber was initially reduced to 0.1 mbar using a rotary pump while it increased to the atmospheric pressure when the test gas is pumped inside.

During this test, the gas concentration was continuously monitored and recorded within the closed chamber at one-second intervals. The gas testing process included the injection of the test gas into the chamber at a constant rate. In the first scenario, measurements were taken without pumping the gas. In the second scenario, gas pumping occurred without the use of the UV source. In the third scenario, we switched the UV source on while the pollutant gas was present to evaluate the photocatalytic effect of the nanocomposite films on the tested gas inside the chamber. All recorded data were saved on the computer for subsequent analysis. The results were compared to the results obtained in previously published articles on the photocatalytic activity of undoped and doped titanium dioxide nanostructures prepared by our research group [15-20,24,25].

 ISSN (print) 2958-8960 (online) 3006-6042 Printed in IRAQ

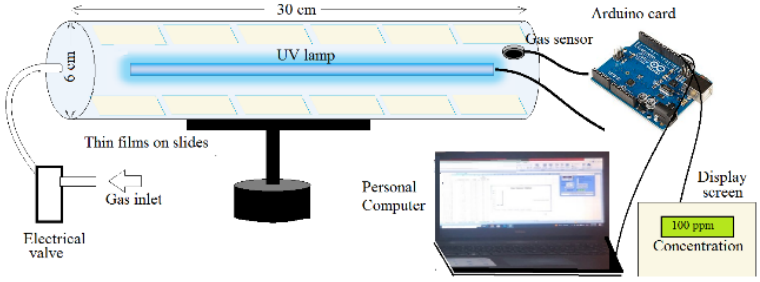

Fig. (1) Scheme of experimental system used for gas purification based on photocatalytic activity assisted with UV source

3. Results and Discussion

Figure (2) illustrates the x-ray diffraction (XRD) pattern of as-deposited TiO_2:TiN nanocomposite thin films. The analysis revealed that the samples exhibited a polycrystalline nature. Upon closer examination, the undoped sample was found to contain a combination of anatase and rutile phases of TiO_2 and TiN, according to JCPDS cards no. 96-900-9087, 96-900-7532, and 96-900-8749, respectively. This observation serves as confirmation of the successful oxidation process of the sputtered substances. In this XRD pattern, a distinct peak indicating a preferred orientation was detected for the predominant anatase phase. This peak was located at diffraction angles (2θ) of 25.39°, corresponding to the (101) crystal plane. The XRD patterns of the composite thin film samples also exhibited a polycrystalline nature. In addition to the anatase and rutile phases observed in the undoped sample, an additional new phase of TiN was observed, characterized by peaks at 36.8340°, 42.7363°, 62.0139°, and 74.2040°, corresponding to the crystal planes of (111), (200), (220), and (311), as defined by JCPDS card no. 96-900-8749.

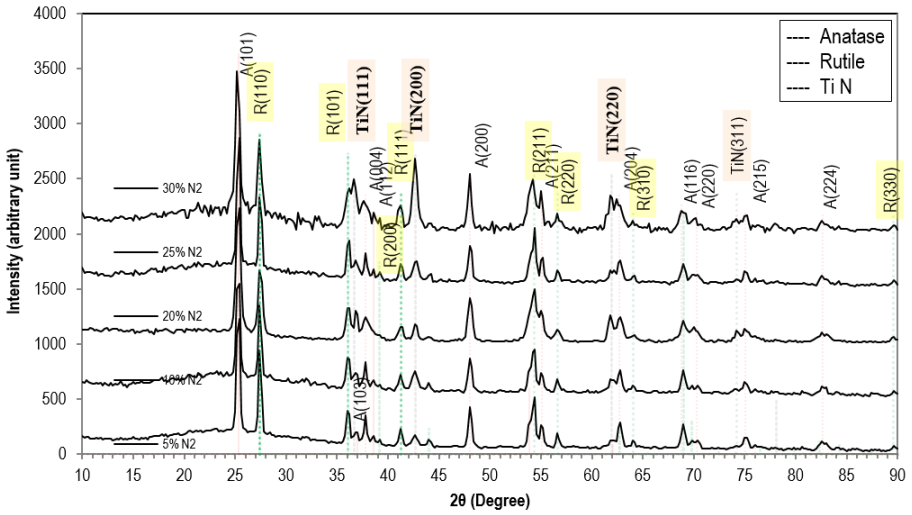

Fig. (2) XRD patterns for TiO_2:TiN composite thin film prepared at different ratios of N_2 in the gas mixture

The FTIR spectra of TiO_2:TiN nanocomposite samples at different gas mixing ratios compared with the TiO_2 film are presented in Fig. (3). These spectra shed light on the distinctive molecular vibrations and chemical interactions within the materials. The band observed at approximately 3410 cm^{-1} is associated with hydroxyl (OH) groups, indicative of surface-bound water molecules. The appearance of the C-H stretching vibration at 2987.24 cm^{-1} corresponds to the adsorption of carbonyl groups (C=O) onto the sample surface. Another significant band is seen at 648.75 cm^{-1}, which indicates vibrations of the TiO_2 matrix [26]. Additionally, a relatively weak band at 423.18 cm^{-1} corresponds to the Ti-O vibration within the rutile crystal structure [27]. An additional band at 1583.00 cm^{-1} is indicative of an intermediate Ti-OH phase, contributing to the presence of defect sites within the TiO_2 matrix. Table (2) lists the FTIR bands for undoped TiO_2 thin film prepared in this work. Upon the introduction of nitrogen (N) in the gas mixture, significant changes manifest within the FTIR spectra as new bands emerge and certain existing bands undergo shifts. A distinctive band arises at 1420 cm^{-1} and increased in intensity with increasing the N content, corresponding to the N-H stretching vibration. Concurrently, bands appearing at 1134.27

cm^{-1}, 1041.96 cm^{-1}, and 1008.39 cm^{-1} are attributed to the presence of Ti-N bonds, unequivocally indicating the formation of TiN phases within the material. Another band at 920.28 cm^{-1} may be attributed to the presence of nitric oxide (NO) or intermediate nitrate phases [28].

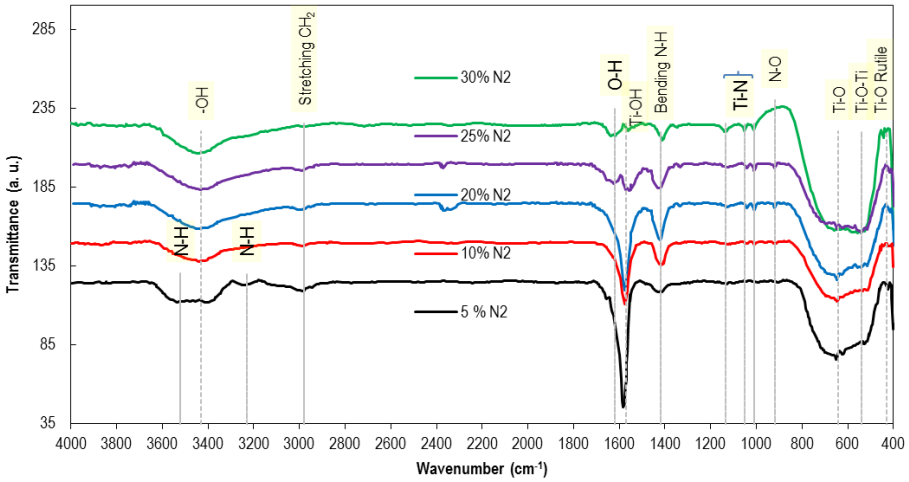

Fig. (3) FTIR spectra for TiO_2 and TiO_2:TiN composite thin films prepared at different ratios of N_2 in the gas mixture

A shoulder band becomes discernible at 540.56 cm^{-1}, indicative of Ti-O-Ti vibrations, further underscoring the structural modifications induced by the doping process. Notably, the appearance and shifting to higher values of these bands affirm the successful incorporation of nitrogen within the TiO_2 matrix, leading to the formation of TiO_2/TiN nanomaterial. These spectroscopic findings contribute valuable information about the nanocomposite's composition, potentially influencing its applicability in diverse technological realms, particularly in photocatalytic applications, owing to the alterations in surface chemistry and defect sites induced by the doping process. Table (1) lists the observed bands in all spectra.

Table (1) FTIR bands for TiO_2 and TiO_2:TiN composite thin films prepared at different N_2 ratios in the gas mixture

Band Type	5% N_2	10% N_2	20% N_2	25% N_2	30% N_2	Reference
N-H	3532.17	-	-	-	-	[25-27]
O-H	3410.49	3427.27	3435.66	3435.66	3439.86	
N-H	3236.36	-	-	-	-	
C-H stretch	2986.71	2986.71	2993.01	2988.81	2978.32	
O-H	-	-	-	1625.17	1627.27	
Ti-OH	1583.22	1576.92	1576.92	1555.94	1562.24	
N-H bending	1421.68	1417.48	1421.68	1427.97	1409.09	
Ti-N	-	-	1134.27	1132.17	1132.17	
	-	1044.06	1041.96	1041.96	1052.45	
	-	1008.39	1008.39	1008.39	1010.49	
N-O	-	916.08	920.28	922.38	-	
Ti-O	648.75	649.55	652.36	655.04	656.75	
Ti-O-Ti	538.46	530.07	540.56	540.56	540.56	
Ti-O rutile	423.18	424.08	425.78	426.69	444.06	

Figure (4) illustrates the absorption spectra of TiO_2/TiN composite thin films. The absorption edge slightly shifts towards longer wavelengths upon increasing of nitrogen (N) ration in the gas mixture and evidently, a noticeable augmentation in absorption is observed across the entire spectral curve following this process. Notably, a broad, elevated feature emerges within the spectrum of the doped sample, spanning from 600 to 750 nm. This feature corresponds to the plasmonic behavior of TiN, signifying its involvement in the absorption phenomena. The absorption characteristics provide crucial insights into the optical properties of the prepared nanomaterials [29]. The observed red-shift in the absorption edge upon adding nitrogen suggests alterations in the electronic structure and bandgap of the composite. Furthermore, the overall enhancement in absorption underscores the potential utility of these materials in harnessing light energy for various applications. The discernible plasmonic response of TiN within the composite sample represents an evident of the extended absorption range, introduces an intriguing avenue for exploiting localized surface plasmon resonances to further enhance the material's

photoresponsive capabilities [30].

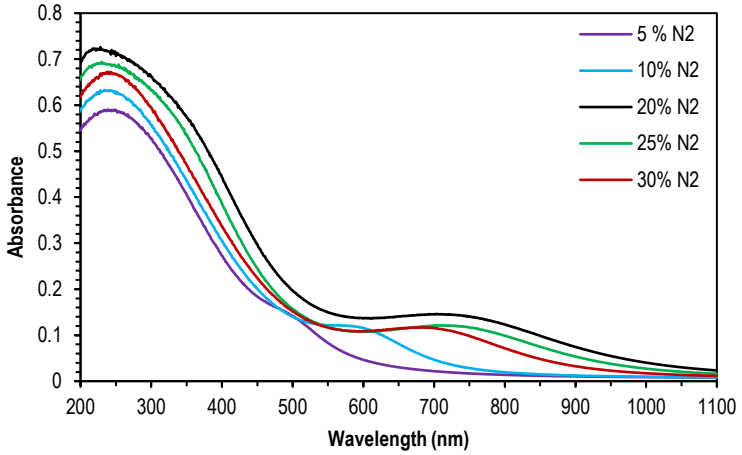

Fig. (4) UV-visible spectra for TiO_2 and TiO_2:TiN composite thin films prepared at different ratios of N_2 in the gas mixture

The optical band gap (E_g^{opt}) for the TiO_2:TiN composite thin films was measured via Tauc's formula by drawing the relation between $(\alpha h\upsilon)^2$ versus $h\upsilon$ as revealed in Fig. (5). The E_g^{opt} decreased gradually from 3.1 eV for 5% N_2 to 2.80 eV with increasing the N_2 flow ratio up to 20% and increased with higher ratio. The decrement in band gap after composing with N due to substitutional doping of N causes the interaction of p states of N-atom with $O_2{}^p$ states [16].

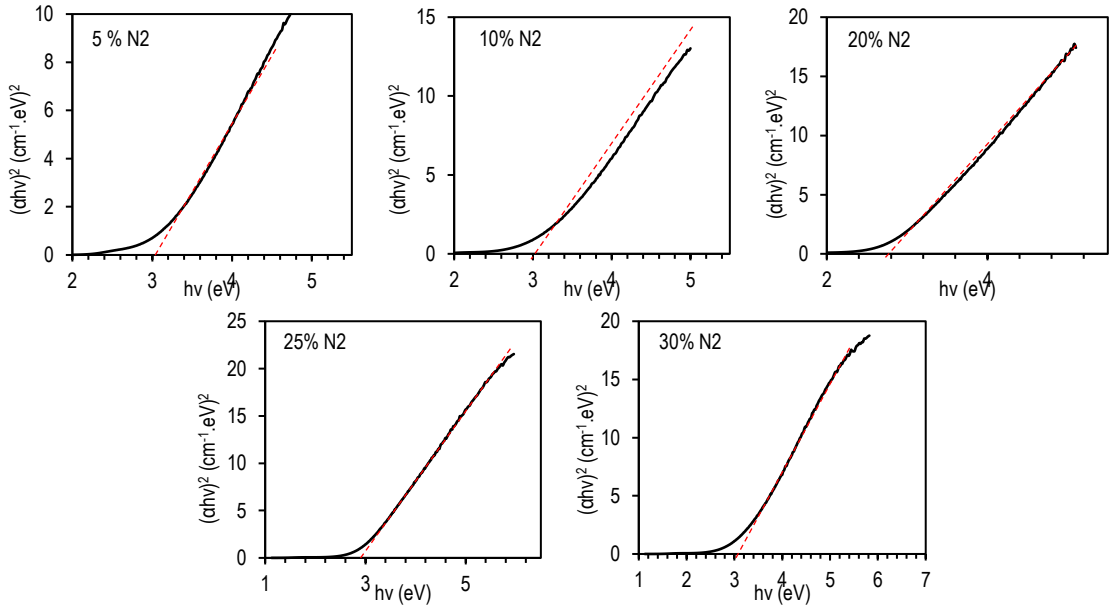

Fig. (5) Relationship between $(\alpha h\upsilon)^2$ and $h\upsilon$ for TiO_2:TiN composite thin films prepared at different ratios of N_2 in the gas mixture

The prepared TiO_2:TiN composite thin film with 20% N_2 was evaluated for its efficacy in the removal of hazardous flammable methane gas. In Fig. (6), we observe the temporal evolution of gas concentration within a closed chamber filled with static air, both before and after the introduction of methane gas. These experiments were conducted with and without the utilization of a UV light source, while the gas interacted with the deposited thin film on glass slides. Initially, a stable gas concentration of 48 parts per million (ppm) was detected in the static air, representing the background level of organic gases prior to the methane pumping. Upon pumping methane gas into the chamber and with the UV source switched off, the gas concentration remained relatively constant at approximately 870 ppm. However, when the UV source was activated, a noticeable decrease in gas concentration occurred over time, eventually reaching a nearly stable value of 200 ppm. This reduction represented a significant

decrease of approximately 79.5% from the initial gas concentration. The removal time required for 90% of the concentration variation was determined to be 44 seconds. This outcome underscores the potential of the composite sample to significantly enhance air quality by efficiently eliminating hazardous flammable gases such as methane.

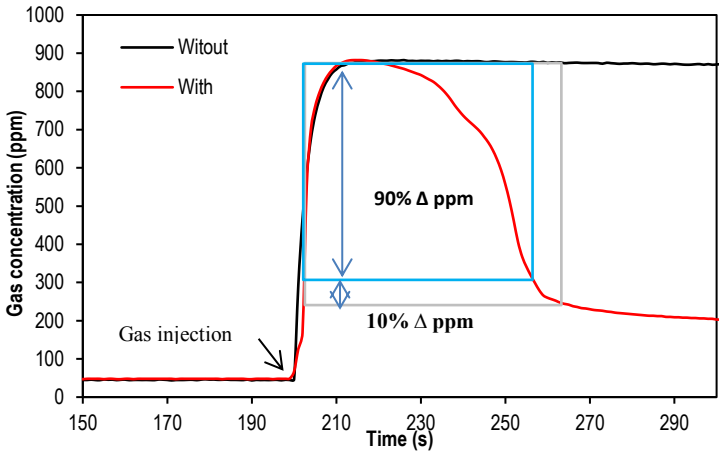

Fig. (6) Air purification test against methane gas based on photocatalytic effect of TiO_2:TiN nanocomposite thin films prepared using 20% N_2 flow ratio

4. Conclusions

TiO_2:TiN nanocomposite thin films were successfully deposited on glass substrates by a dc reactive magnetron sputtering technique. The structural, morphological, and optical properties of the as deposited samples indicate the successful formation of this composite material. The results show the distinct variations in thin film properties with the N content in the gas mixture. This work explores the fascinating potentials of TiO_2 thin films prepared by dc reactive sputtering, highlighting their transformation and remarkable enhancement in the UV-visible absorption and red-shifted edge upon compositional modification with nitrogen (N_2) at various ratios to harness much more light. The prepared TiO_2:TiN nanocomposites are efficient for air purification, specifically show high efficiency in the removal of methane gas with the assistance of a UV light source.

References

[1] H. Yang et al., Catalysts 12(10), 1263 (2022).
[2] C.H.A. Tsang et al., Enviro. Int., 125, 200–228 (2019).
[3] D. Reyes-Coronado et al., Nanotech., 19(14), 145605 (2008).
[4] M. Shahiduzzaman et al., Nano-Micro Lett., 13(1), 36 (2021).
[5] Q. Zheng, X. Zhang, and X. Zhou, Int. J. Ener. Res., 44(7), 6035–6048 (2020).
[6] S.C. Ray et al., J. Phys. Chem. C, 126(20), 8947–8952 (2022).
[7] L. Mekala et al., Appl. Mech. Mater., 903, 51–56 (2021).
[8] "Deposition Technologies," in *Handbook of Deposition Technologies for Films and Coatings* (Elsevier, 2010), pp. 1–31.
[9] K. Eufinger et al., J. Phys. D: Appl. Phys., 40(17), 5232–5238 (2007).
[10] N. Madkhali et al., Result. Eng., 17, 100920 (2023).
[11] B. Naufal, S. G. Ullattil, and P. Periyat, Solar Energy 155, 1380–1388 (2017).
[12] L.O.A. Salim et al., J. Phys. Chem. Solids, 175, 111224 (2023).
[13] M. Pavel et al., Catalysts 13(2), 380 (2023).
[14] S.J. Armaković, M.M. Savanović, and S. Armaković, Catalysts 13(1), 26 (2022).
[15] O.A. Hammadi, F.J. Kadhim and E.A. Al-Oubidy, Nonl. Opt. Quantum Opt., 51(1-2) (2019) 67-78.
[16] F.J. Al-Maliki, O.A. Hammadi and E.A. Al-Oubidy, Iraqi J. Sci., 60(special issue) (2019) 91-98.
[17] E.A. Al-Oubidy and F.J. Al-Maliki, Opt. Quantum Electron., 51(1-2) (2019) 23.
[18] F.J. Al-Maliki et al., Opt. Quantum Electron., 52 (2020) 188.
[19] F.J. Al-Maliki and M.A. Al-Rubaiy, Opt. Quantum. Electron., 54 (2022) 377.
[20] Z.H. Zaidan, O.A. Hammadi and K.H. Mahmood, Iraqi J. Appl. Phys., 19(3A) (2023) 55-58.
[21] C. Thambiliyagodage, Enviro. Nanotech. Monitor. Manag., 16, 100592 (2021).
[22] B. Liu, L. Wen, and X. Zhao, Sol. Ener. Mater. Solar Cells, 92(1), 1–10 (2008).
F.J. Al-Maliki and E.A. Al-Oubidy, Physica B: Cond. Matter, 555 (2019) 18-20
[23] F.J. Kadhim, O.A. Hammadi and N.H. Mutesher, J. Nanophot., 16(2) (2022) 026005 DOI: 10.1117/1.JNP.16.026005
[24] C. Afonso et al., J. Phys.: Conf. Ser., 2407(1), 012001 (2022).
[25] P. Kumar et al., Adv. Opt. Mater., 8(4), 1901275 (2020).
[26] R. Singh, M. Gupta, and S.K. Mukherjee, J. Mater. Sci.: Mater. Electron., 33(9), 6942–6953 (2022).
[27] U. Guler et al., Nanophotonics 4(3), 269–276 (2015).